

# Intermolecular potential and second virial coefficient of the water–helium complex

Matthew P. Hodges<sup>a)</sup> and Richard J. Wheatley

*School of Chemistry, University of Nottingham, University Park, Nottingham, NG7 2RD, United Kingdom*

Allan H. Harvey

*Physical and Chemical Properties Division, National Institute of Standards and Technology, Boulder, Colorado 80305*

(Received 22 August 2001; accepted 2 October 2001)

A potential-energy surface for the water–helium complex is constructed from scaled perturbation theory calculations, and calibrated using accurate supermolecule methods. At the global minimum, the helium atom lies in the plane of the water molecule with an interaction energy corresponding to about  $35 \text{ cm}^{-1}$  ( $-160$  microhartree). The potential is used to calculate second virial coefficients, including first-order quantum corrections, from 100 to 2000 K. The estimated uncertainties in the calculated values are much smaller than the uncertainties in the available experimental data; the calculated values also cover a much wider range of temperature. The quantum corrections are found to be smaller in magnitude than the uncertainty in the calculated second virial coefficient. © 2002 American Institute of Physics. [DOI: 10.1063/1.1421065]

## I. INTRODUCTION

The development of accurate intermolecular potentials for weakly bound van der Waals complexes using supermolecule *ab initio* methods still represents a significant commitment of computational resources. When dispersion forces dominate, Gaussian basis sets with both diffuse and high angular momentum functions are required along with sophisticated treatments of electron correlation. The potential-energy surface also represents a fine balance between long-range forces and the short-range exchange-repulsion interactions, and a good account of the latter contribution is crucial if spectroscopic accuracy is to be approached.

In previous work on the  $\text{NH}_3 \cdots \text{He}$  complex,<sup>1</sup> we demonstrated that scaled perturbation theory (PT) methods were capable of recovering accurate supermolecule interaction energies at a fraction of the computational cost. We now turn our attention to  $\text{H}_2\text{O} \cdots \text{He}$ , which represents the start of a program of research on complexes of water combined with rare-gas atoms and molecules abundant in the atmosphere. There has been previous interest in the  $\text{H}_2\text{O} \cdots \text{He}$  system. Tao *et al.*<sup>2</sup> used fourth-order Møller–Plesset (MP4) theory with an  $\text{O}(7s5p3d)/\text{H}(5s2p)/\text{He}(6s3p)$  basis plus bond functions to survey the potential-energy surface. The global minimum was estimated, at this level of theory, to have an interaction energy of about  $-144.9 \mu E_h$  ( $E_h \approx 4.359\,744 \times 10^{-18} \text{ J}$ ) and the correct value was estimated to be about  $-154.9 \mu E_h$ . Earlier calculations by Green and co-workers<sup>3,4</sup> employed a fitted surface derived from MP4 data to calculate pressure broadening of microwave lines for  $\text{H}_2\text{O}$  in He. The potential from Ref. 3 has also been used to investigate surface vibrations of water clusters, probed by helium scattering experiments.<sup>5</sup>

The thermodynamic properties of gaseous mixtures containing water are also of interest to the industrial community. In the heating, ventilation, and air conditioning (HVAC) industries, the properties of moist air are important design data, and a standard formulation exists<sup>6</sup> for a limited range of conditions. Combustion turbines are attaining widespread use in the power industry; better knowledge of the properties of combustion gases would aid in their design and optimization. An accurate description of the nonideality of water-air mixtures is essential for the development of humidity standards.<sup>7</sup> The properties of moist air are also important for precision metrology; for example, the density of the ambient air is needed to make buoyancy corrections in weighing<sup>8</sup> and its refractive index is required for length measurement by interferometry.<sup>9</sup>

In most of these applications, the pressures of interest are not high, ranging from one to perhaps twenty times normal atmospheric pressure. The resulting densities are such that an appropriate level of thermodynamic description is that of the second virial coefficient, the first correction to ideal-gas behavior. A description in terms of second virial coefficients has the advantage that the thermodynamics of a multicomponent mixture can be calculated rigorously given only the temperature-dependent second virial coefficients  $B_{ij}(T)$  for all pairs of species in the system.

Unfortunately, few reliable data exist for  $B_{ij}$  where one component is water. The usual techniques to extract  $B_{ij}$  from gas-phase pressure-volume-temperature measurements are ruined (or at best made much more difficult) by adsorption on the surfaces of the apparatus at temperatures below roughly 500 K.<sup>10</sup> Values can be backed out from measurements of the solubility of ice or liquid water in a gas, but these experiments are limited in the temperature range that can be covered and typically produce second virial coefficients with large uncertainties. On the other hand,  $B_{ij}(T)$  can

<sup>a)</sup>Author to whom correspondence should be addressed. Electronic mail: pczmph@unix.nott.ac.uk

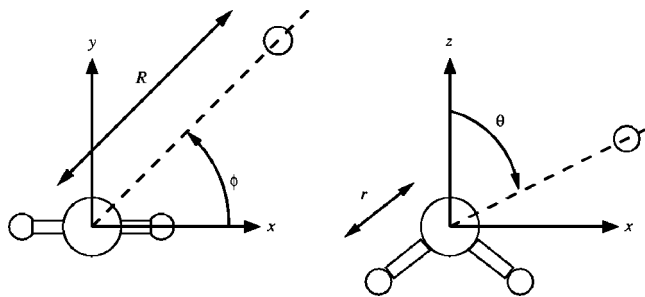


FIG. 1. Coordinate system used to describe the  $\text{H}_2\text{O}\cdots\text{He}$  complex. The origin is at the oxygen atom. The position of the helium atom is described by the spherical polar coordinates  $R$ ,  $\theta$  and  $\phi$ .

be calculated rigorously from statistical mechanics if the intermolecular potential  $U(r_{ij}, \Omega_i, \Omega_j)$  is known (here  $r_{ij}$  is the vector between molecules  $i$  and  $j$  and  $\Omega_i$  and  $\Omega_j$  represent their orientations). High-quality pair potentials for aqueous systems may therefore produce second virial coefficients with accuracy and precision superior to experimentally obtained values.

One of us<sup>11</sup> recently compared the experimental second virial coefficient of pure water with theoretical predictions using a state-of-the-art potential from the literature. In this case,  $B(T)$  is known fairly accurately above about 350 K (because for a pure substance one does not have to rely solely on the adsorption-prone experiments), and the second virial coefficients calculated from the pair potential were unable to match the data below about 500 K. This was attributed to higher-order rotational quantum corrections to  $B(T)$  that could not be computed. However, for the water-gas binaries of interest to us here, these rotational corrections should be less important, because they depend on the intermolecular torques, which are expected to be smaller for these less anisotropic systems. In addition, the experimental  $B_{ij}(T)$  are known much less accurately for these mixtures than for pure water, so calculations from an intermolecular potential will not have to be so accurate in order to provide an improvement over existing experimental results.

## II. METHODS

The methods used in this work are similar to those used for the  $\text{NH}_3\cdots\text{He}$  intermolecular potential from Ref. 1, where scaled PT calculations were used to characterize the potential-energy surface as a function of the inversion tunneling coordinate. To avoid excessive repetition, we therefore give only an outline here, and highlight specific differences that arise.

### A. Sampling the potential-energy surface

The coordinate system used is shown in Fig. 1. The bond length and bond angle for water are those recommended by Mas and Szalewicz,<sup>12</sup> i.e.,  $r = 1.8361 a_0$  ( $a_0 \approx 0.05291772$  nm) and  $\angle\text{HOH} = 104.69^\circ$ , which correspond to vibrationally averaged ground-state monomer coordinates. The water monomer is kept rigid and the intermolecular coordinates describing the location of helium ( $R$ ,  $\theta$  and  $\phi$ ) are sampled to give configurations at which to evaluate the interaction energy:  $R$  is varied from 3 to  $8 a_0$  in  $1 a_0$  incre-

ments and 256 symmetry-distinct orientations are chosen using a two-dimensional Sobol sequence<sup>13</sup> to sample the angles  $\theta$  and  $\phi$ . This yields a total of 1536 points.

### B. Perturbation theory calculations

At each configuration on the potential-energy surface, the total PT interaction energy is calculated (using aug-cc-pVQZ basis sets<sup>14,15</sup>) as the sum of induction, dispersion, penetration, and exchange-repulsion contributions:

$$\Delta E(\text{PT}) = E_{\text{ind}} + E_{\text{disp}} + E_{\text{pen}} + E_{\text{exch}}. \quad (1)$$

The induction and dispersion energies are calculated using the random-phase approximation (RPA) using the usual second-order PT expressions. The leading term in the multipolar induction energy of helium is proportional to the square of the  $\text{H}_2\text{O}$  dipole moment multiplied by the polarizability of He.<sup>16</sup> The square of the experimental dipole moment of  $\text{H}_2\text{O}$  is 0.86335 times the Hartree-Fock self-consistent field (SCF) value and the polarizability of He is 1.0484 times our RPA value. These induction energies are hence scaled by 0.9051. The induction energies of  $\text{H}_2\text{O}$ , which have no multipolar component and are much smaller, are not scaled. In our previous work,<sup>1</sup> we scaled the dispersion energies isotropically by the ratio of experimental to RPA  $C_6$  coefficients such that

$$C_N = \alpha \times C_N^{\text{RPA}}, \quad (2)$$

where  $\alpha$  is a dimensionless scaling factor. This ensures that the long-range asymptotic form of the potential (i.e., the  $R^{-6}$  behavior) is correct. However, because the effects of basis set incompleteness and electron correlation are expected to increase with  $N$ , we refine this method by introducing a second scaling parameter and use

$$C_N = \alpha \times k^{(N-6)} \times C_N^{\text{RPA}}. \quad (3)$$

This requires the  $C_N$  to be calculated at each orientation; the damping functions,  $f_N(bR)$ , also need to be determined. The multipolar dispersion energy coefficients with  $6 \leq N \leq 14$  are calculated directly from the ground and excited states in the RPA approximation. The damping functions are assumed to have the Tang-Toennies form,<sup>17</sup> and the scale parameter,  $b$ , is fitted separately at each point on the potential-energy surface. Clearly Eq. (3) still results in the correct long-range  $R^{-6}$  behavior. Moreover, this method does not require that the damping functions have the correct  $R$ -dependence, since  $b$  is free to vary with  $R$ . The experimental  $C_6$  is  $8.000 E_h a_0^6$ <sup>18</sup> and our RPA value is  $7.388 E_h a_0^6$  leading to  $\alpha = 1.083$ ; we will return to the determination of  $k$  below.

Correlated monomer charge densities at the quadratic configuration interaction with single and double substitutions (QCISD) and SCF levels of theory are obtained with the GAUSSIAN 94 program<sup>19,20</sup> and used by the GMUL program<sup>21</sup> to calculate QCISD penetration (Coulomb) energies and SCF and QCISD charge-density overlap integrals. Heitler-London first-order exchange-repulsion energies are then calculated and scaled by the ratio of the QCISD and SCF charge-density overlaps to give approximate correlated exchange-repulsion energies.<sup>22</sup>

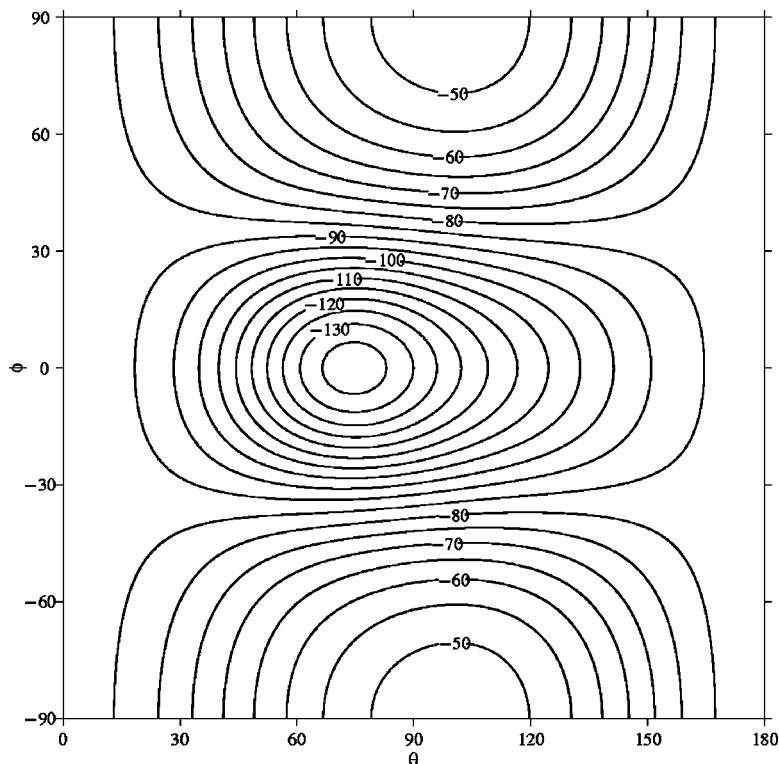


FIG. 2. Potential-energy surface for the initial parametrization of the perturbation theory data (Surface I; see text for details). The angles  $\theta$  and  $\phi$  are given in degrees, the energy contours in  $\mu E_h$ .

### C. Fitting the potential-energy surfaces

The sum of the induction and dispersion interaction energies is fitted to a damped multipolar series of the form

$$E_{\text{ind}} + E_{\text{disp}} = - \sum_a \sum_n C_{na} R_a^{-n} f_n(\beta R_a), \quad (4)$$

where  $a$  represents the three nuclei of water,  $R_a$  is the distance from the helium nucleus to nucleus  $a$ , the integer  $n$  takes values 6, 8 and 10,  $f_n(\beta R_a)$  is a Tang-Toennies damping function and  $\beta$  is a fitted parameter. The coefficient  $C_{na}$  is assumed to be independent of the position of the helium atom when  $a$  is a hydrogen nucleus, but when  $a$  is the oxygen nucleus, anisotropy is introduced by expanding the  $C_{na}$  in spherical harmonics:

$$C_{na} = \sum_{lm} C_{na,lm} F_{lm}(\theta, \phi). \quad (5)$$

All symmetry-allowed  $l \leq 5$  terms are used such that there are 12 independent  $C_{na,lm}$  coefficients for each  $n$ . In total there are therefore 39  $C$  parameters (3 on hydrogen and 36 on oxygen); these are fitted by minimizing the Boltzmann-weighted error,

$$W^2 = \sum_g w_g \times (E_{\text{fit}}(g) - E_{\text{calc}}(g))^2 / \sum_g w_g, \quad (6)$$

where  $g$  includes all 1536 geometries,  $E_{\text{fit}}$  is the fitted function [the right-hand side of Eq. 4 in this case],  $E_{\text{calc}}$  is the calculated energy (sum of induction and dispersion energies) and the weights are given by

$$w_g = \exp(-(\Delta E(\text{PT})(g) - E_0)/E_d), \quad (7)$$

where  $\Delta E(\text{PT})$  is the total calculated interaction energy (including exchange-repulsion and penetration),  $E_0 = -150 \mu E_h$  and  $E_d = 3 \text{ m}E_h$  (about 950 K). The weighting parameters  $E_0$  and  $E_d$  are chosen to ensure that repulsive configurations sampled at temperatures up to 2000 K are given adequate weights in the fit;  $E_0$  is approximately the potential-energy minimum. The fitting procedure is insensitive to  $\beta$  and a value of  $3.7 a_0^{-1}$  is chosen.

The fitted long-range energies are then subtracted from the corresponding calculated total interaction energies to give a set of “adjusted” short-range energies,  $E_{\text{sr}}$ , to be fitted. These differ slightly from the calculated exchange-repulsion plus penetration energies, because of the error in fitting the long-range energies. The short-range energies are fitted using the function

$$E_{\text{sr}} = \sum_a (A_{0a} + A_{1a} R_a + A_{2a} R_a^2) \exp(-\zeta R_a). \quad (8)$$

When  $a$  is a hydrogen nucleus, each  $A$  parameters is a sum of three terms:

$$A_{na} = A_{na}^0 + A_{na}^1 Z'/R_a + A_{na}^2 (3(Z'/R_a)^2 - 1), \quad (9)$$

where  $Z'/R_a$  is the cosine of the angle between the H→O and H→He vectors. When  $a$  is the oxygen nucleus, each  $A$  parameter is a sum of twelve terms and each  $A_{na}$  term is expanded in spherical harmonics as in Eq. (5). There are therefore 45  $A$  coefficients in the fit plus the non-linear parameter  $\zeta$ , which is fixed at  $1.70 a_0^{-1}$ . Equation (6) is used with the weighting parameters given above to fit the adjusted short-range data. A number of sets of data are fitted in this

TABLE I. Details of stationary points on the first fitted potential-energy surface (Surface I). The angles  $\theta$  and  $\phi$  are given in degrees,  $R$  in  $a_0$ . The fitted energies are given in  $\mu E_h$  along with single point CCSD(T)/aug-cc-pVQZ energies at the same geometries.

$R$	$\theta$	$\phi$	$\Delta E$	
			Surface I	CCSD(T)/aug-cc-pVQZ
5.95	74.5	0.0	-137.8	-150.8
6.27	0.0	0.0	-87.2	-93.6
6.79	180.0	0.0	-83.1	-94.6
7.02	99.9	90.0	-46.5	-58.2

way (see Secs. III A to III C), and in each case the errors in the long-range and short-range fits are always less than  $W = 2 \mu E_h$ .

#### D. Supermolecule calculations

Stationary points on the fitted potential-energy surfaces are compared with *ab initio* supermolecule calculations. All of these have been performed using Molpro<sup>23</sup> with aug-cc-pVXZ basis sets<sup>14,15</sup> up to 5- $\zeta$  quality (i.e., X=D, T, Q, 5). The coupled-cluster method with single, double and perturbative triple substitutions [CCSD(T)] is used to calculate interaction energies employing the full counterpoise correction method<sup>24</sup> throughout.

#### E. Calculation of the second virial coefficient

The second virial coefficient for the water–helium complex,  $B_{12}(T)$ , is evaluated using standard methods (see e.g., Gray and Gubbins<sup>25</sup>); for convenience we drop the 12 label for the calculated components of  $B_{12}(T)$ . The classical component is evaluated as the integral of the Mayer function over all space:

$$B_{\text{class}}(T) = -\frac{1}{2} \int \langle \exp(-U_{12}/k_B T) - 1 \rangle_{\Omega_1, \Omega_2} d\mathbf{R}, \quad (10)$$

where  $U_{12}$  is the pair potential and  $\langle \dots \rangle_{\Omega_1, \Omega_2}$  represents averaging over all molecular orientations. At lower temperatures, quantum effects become important for systems with small masses or small moments of inertia. A semi-classical expansion in orders of  $\hbar^2$  yields first-order translational and rotational corrections given by

$$B_{\text{quant}}^{\text{trans}}(T) = \frac{\hbar^2}{24(k_B T)^3} \times \frac{\langle \mathbf{F}^2 \rangle_0}{2M_r} \quad (11)$$

$$B_{\text{quant}}^{\text{rot}}(T) = \frac{\hbar^2}{24(k_B T)^3} \times \sum_{\alpha=x,y,z} \frac{\langle T_\alpha^2 \rangle_0}{I_\alpha}, \quad (12)$$

where  $\mathbf{F}$  is the force on each molecule,  $M_r$  is the reduced mass of the system and  $T_\alpha$  the torque about local molecular axis  $\alpha$  with moment of inertia  $I_\alpha$ . The  $\langle \dots \rangle_0$  notation represents integration weighted according to the zero-density pair distribution function. The rotational correction for this mixed system is taken as the average of the two fragment contributions; since there is no contribution from He, the total is half the amount calculated for  $\text{H}_2\text{O}$ . The total

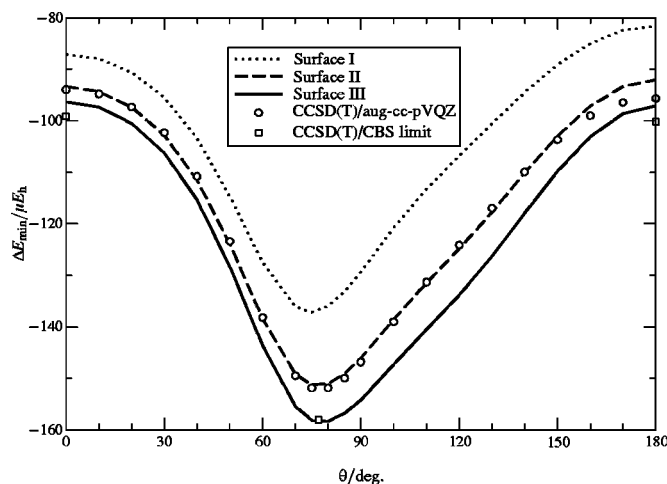


FIG. 3. One-dimensional cut through potential-energy surfaces with  $\phi=0$ . For each value of  $\theta$ , the energy plotted,  $\Delta E_{\text{min}}$ , is the minimum with respect to varying  $R$ .

quantum-corrected second virial coefficient,  $B_{\text{tot}}(T)$ , is defined as the sum of the contributions from Eqs. (10)–(12).

### III. POTENTIAL-ENERGY SURFACES

We discuss results for a number of surfaces that we have developed using the scaling methods outlined in Sec. II B. All use the same scaling procedure for the exchange-repulsion and induction energies, and therefore differ only in the determination of the dispersion energy.

#### A. Initial parametrization of the potential-energy surface

The first fitted surface that we report (Surface I) uses isotropic scaling of the dispersion energies, i.e., Eq. (2). A two-dimensional cut through this surface in  $\theta$  and  $\phi$  is shown in Fig. 2, where, for each orientation, the interaction energy has been minimized with respect to  $R$ . The global (and in fact only) minimum on the surface has the helium atom in the plane of the molecule ( $\phi=0$ ) at about  $\theta=74.5^\circ$  and  $R=5.95 a_0$ . The interaction energy is about  $-137.8 \mu E_h$ . Axial transition states occur at  $\theta=0$  and  $\theta=180^\circ$  at energies of  $-87.2$  and  $-83.1 \mu E_h$ , respectively; the most facile rearrangement between the two versions of the global minimum therefore involves the helium atom remaining in the plane of the molecule and moving around the oxygen atom. A third transition state at  $\theta=99.9^\circ$  and  $\phi=90^\circ$  with an interaction energy of  $-46.5 \mu E_h$  corresponds to out-of-plane motion of the helium around the molecule with a somewhat larger energy barrier. The location of the minimum reflects a balance between maximizing the dispersion interaction and reducing the repulsion between helium and the lone pairs of electrons on the water molecule.

The energies and geometries of these stationary points are collected in Table I with single-point CCSD(T)/aug-cc-pVQZ energies at the same geometries. Qualitative agreement is seen, though it is apparent that there is some deficiency in the scaling method used; the fitted surface captures about 90% of the *ab initio* interaction energy. The exchange-repulsion and penetration components are expected to be

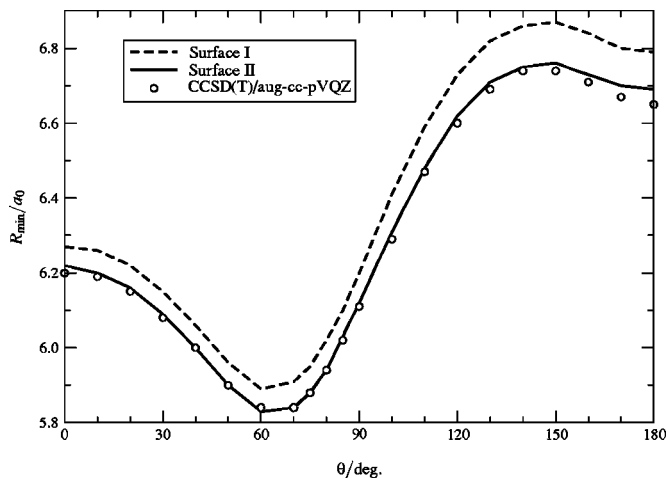


FIG. 4. One-dimensional cut through potential-energy surfaces with  $\phi = 0$ . For each value of  $\theta$ , the value of  $R$  at the energy minimum,  $R_{\min}$ , is shown.

more accurate than the induction and dispersion contributions, and since the former of these is small, we attribute the discrepancies to insufficient scaling of the higher-order  $C_N$ .

## B. Refinement of the potential-energy surface

To determine an improved set of long-range energies, we scale the dispersion coefficients using Eq. (3), and this requires determination of the  $k$  parameter. To investigate this, we have calculated scaled PT and CCSD(T)/aug-cc-pVQZ interaction energies on a two-dimensional cut through the potential-energy surface with  $\phi = 0^\circ$ , including the minimum and two axial stationary points. Calculations were performed at  $\theta = 0-180^\circ$  in  $10^\circ$  increments with additional points near the minimum at  $\theta = 75$  and  $85^\circ$ . A grid of  $R$  was sampled, and for each  $\theta$  the minimum energy as a function of  $R$  was determined by assuming an  $\exp -6$  form, finding the optimal potential parameters from a Boltzmann-weighted r.m.s. fit with  $k_B T = 30 \mu E_h$  ( $T = 9.5$  K) and minimizing the fitted function with respect to  $R$ . A value of  $k = 1.05$  approximately reproduces the CCSD(T)/aug-cc-pVQZ minimum close to  $\theta = 80^\circ$ , and this scaling leads to Surface II. The *ab initio* and scaled PT data for Surfaces I and II are plotted in Fig. 3. (Surface III and the CCSD(T)/CBS calculations are defined below in Sec. III C.) It is apparent that the more sophisticated scaling of the dispersion energies leads to a surface that quantitatively recovers the *ab initio* results. It is important to realize that the parameter  $k$  was determined solely to repro-

TABLE II. Details of stationary points on the second fitted potential-energy surface (Surface II). The angles  $\theta$  and  $\phi$  are given in degrees,  $R$  in  $a_0$ . The fitted energies are given in  $\mu E_h$  along with single point CCSD(T)/aug-cc-pVQZ energies at the same geometries.

$R$	$\theta$	$\phi$	$\Delta E$	
			Surface II	CCSD(T)/aug-cc-pVQZ
5.91	77.0	0.0	-152.1	-152.1
6.22	0.0	0.0	-93.7	-94.0
6.70	180.0	0.0	-93.6	-95.7
6.93	99.1	90.0	-50.8	-59.3

TABLE III. Details of stationary points on the third fitted potential-energy surface (Surface III). The angles  $\theta$  and  $\phi$  are given in degrees,  $R$  in  $a_0$ . The fitted energies are given in  $\mu E_h$  along with single point complete basis set (CBS) estimates at the CCSD(T) level at the fitted Surface II stationary points.

$R$	$\theta$	$\phi$	$\Delta E$	
			Surface III	CCSD(T)/CBS estimate
5.90	78.3	0.0	-159.2	-158.2
6.19	0.0	0.0	-96.7	-99.2
6.66	180.0	0.0	-98.7	-100.2
6.90	98.7	90.0	-52.8	-63.1

duce the well depth, but that the potential-energy surface is extremely well approximated for almost the entire range of  $\theta$  (with only minor discrepancies for  $\theta > 150^\circ$ ). This is strong evidence that the scaling procedure we have chosen is physically sound, and further support for this can be seen in a plot of the optimal O-He separations,  $R_{\min}$ , for each value of  $\theta$  (Fig. 4). The CCSD(T)/aug-cc-pVQZ results are reproduced well by Surface II (again with larger discrepancies at large  $\theta$ ).

Stationary points for the fitted Surface II data have been located and are compared with single point CCSD(T)/aug-cc-pVQZ calculations in Table II. The near perfect agreement between the fitted and *ab initio* interaction energies at the minimum is obtained by the choice of  $k$ . The two axial stationary points are nearly degenerate on the fitted surface compared with an energy difference of about  $2 \mu E_h$  in the *ab initio* calculations. The equatorial stationary point, the highest in energy, is the least well represented, and here the error in the energy is about  $8.5 \mu E_h$ . The cut through Surface II with  $\phi = 90^\circ$ , i.e., that containing the axial and equatorial transition states, does not reproduce the CCSD(T)/aug-cc-pVQZ data as well. This pathway involves the helium atom moving in the plane containing the lone pairs, and further refinement of the scaling procedure, e.g., using an anisotropic function in place of  $k$  in Eq. (3), may be required to improve this region of the potential-energy surface. We note, however, that fourth-order Møller-Plesset calculations with single, double, triple, and quadruple substitutions [MP4(SDTQ)] using the same basis set give less negative interaction energies than at the CCSD(T) level.

## C. Calibration with complete basis set limit estimates

So far we have shown that judicious scaling of PT calculations can result in a potential-energy surface comparable with high-quality supermolecule data, although at a fraction of the computational cost. We now try to account for the incompleteness of the basis set used in our calculations. We proceed as for Surface II, except that we adjust  $k$  from Eq. (3) to approximate a single complete basis set (CBS) limit calculation. We have taken the geometry of the minimum from the fitted Surface II and calculated a single point CCSD(T)/aug-cc-pV5Z energy there. Assuming that the interaction energy approaches the CBS limit exponentially as a function of the cardinal basis set index (i.e.,  $X$  in aug-cc-pVXZ), we estimate the CBS limit at the Surface II mini-

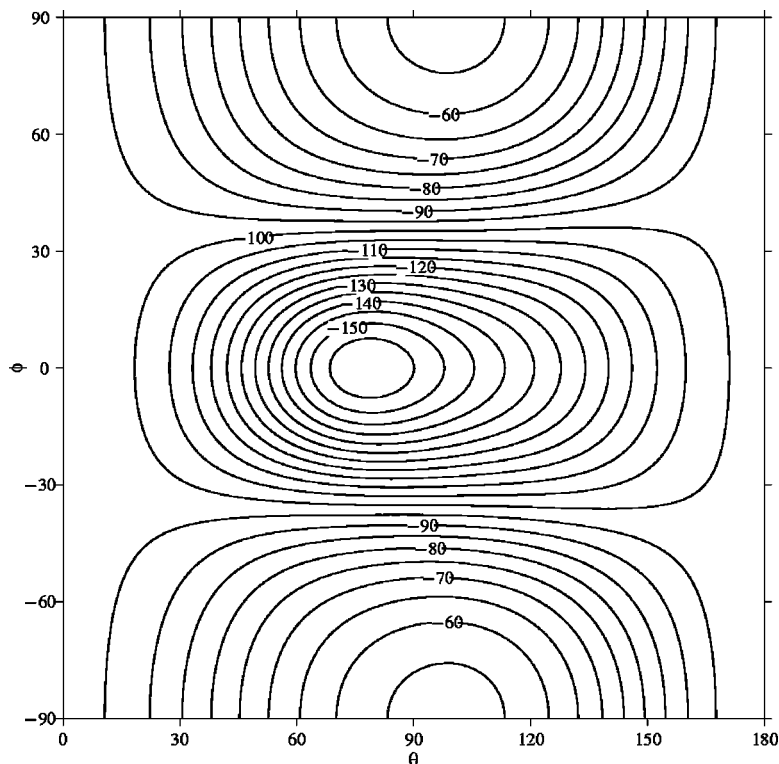


FIG. 5. Potential-energy surface for the third parametrization of the perturbation theory data (Surface III; see text for details). The angles  $\theta$  and  $\phi$  are given in degrees, the energy contours in  $\mu E_h$ .

imum to be about  $-158 \mu E_h$ . (This assumption is supported by two observations: (1) the CBS limit is insensitive to removing the X=5 point and (2) using X=D-Q, the estimated X=5 energy is in error by only  $0.3 \mu E_h$ .) This procedure leads to  $k=1.07$ , and this value is used to define Surface III. The energies of the four fitted Surface III stationary points are compared with the CBS estimates in Table III (see also Fig. 3); it was not deemed necessary to perform CBS estimates at the Surface III stationary points due to the similarity of the Surface II and Surface III geometries. The minimum energy is reproduced to within about  $1 \mu E_h$ ; again this good agreement is due to the choice of  $k$ . The axial stationary points have slightly larger errors, and the equatorial transition state is least well accounted for (as discussed in Sec. III B previously).

Surface III represents our best estimate of the  $\text{H}_2\text{O}\cdots\text{He}$  intermolecular interaction, and a contour plot is shown in Fig. 5. Qualitatively there is little difference between Surfaces II and III, the latter being globally deeper. The PT components calculated at the Surface III stationary points are given in Table IV. Clearly the dispersion dominates the attractive components, though penetration and induction collectively contribute about 15–20% to the total attractive en-

TABLE IV. Perturbation theory components of the interaction energy, in  $\mu E_h$ , using the Surface III scaling method at the fitted Surface III stationary points.

$E_{\text{exch}}$	$E_{\text{pen}}$	$E_{\text{ind}}$	$E_{\text{disp}}$	$\Delta E(\text{PT})$
211.7	-38.9	-22.5	-309.7	-159.3
125.3	-23.3	-21.9	-176.6	-96.6
134.9	-25.6	-13.9	-193.0	-97.7
76.6	-14.7	-5.6	-109.2	-52.9

ergy. In fact the relative contributions from dispersion and penetration are reasonably consistent for all four stationary points, the induction energy varying slightly more. Our best estimate for the interaction energy of  $-158 \mu E_h$  lies below the estimate of Tao *et al.*<sup>2</sup> of  $-155 \mu E_h$ , even though our value does not account for correlation effects missing from the CCSD(T)/CBS calculation. The FORTRAN source for the fitted Surface III is available via EPAPS as supplementary material.<sup>26</sup>

We note that this estimate of the interaction energy is very close to the value of  $-153 \mu E_h$  that we reported for  $\text{NH}_3\cdots\text{He}$ .<sup>1</sup> In this case, the minimum is at  $\phi=60^\circ$  (the coordinate system is defined with one H atom in the  $xz$  plane, with  $x>0$ ) such that the He atom is staggered between the two closest H atoms. A somewhat larger interaction energy of about  $-181 \mu E_h$  has been reported for the  $\text{HF}\cdots\text{He}$  complex<sup>27</sup> for a linear configuration with He at the H end of the molecule. For each of these three complexes, the minimum-energy configuration can be understood to arise from maximizing the attractive intermolecular interactions, subject to the constraint of the rare-gas atom avoiding the lone pairs. Also of interest are the trends for the series of  $\text{H}_2\text{O}$  interacting with He, Ne, and Ar. The minimum in each case is planar, and an interaction energy of about  $-206 \mu E_h$  has been reported for  $\text{H}_2\text{O}\cdots\text{Ne}$  by Bagno<sup>28</sup> using MP2 calculations; an interaction energy of about  $-651 \mu E_h$  has been determined for  $\text{H}_2\text{O}\cdots\text{Ar}$  from the AW2 potential of Cohen and Saykally,<sup>29</sup> which was fitted to reproduce a range of spectroscopic data. Our own preliminary calculations on  $\text{H}_2\text{O}\cdots\text{Ne}$ <sup>30</sup> at the CCSD(T)/aug-cc-pV5Z level indicate that the interaction is significantly stronger than reported in Ref. 28, at about  $-300 \mu E_h$ .

## IV. SECOND VIRIAL COEFFICIENTS

### A. Experimental second virial coefficients

For the water-helium pair, it appears that the only experimental data from which one can extract second virial coefficients are measurements by Iomtev *et al.*<sup>31</sup> of the solubility of ice in helium gas. Since these data were not converted to second virial coefficients in the original work, we briefly describe the conversion procedure.

We begin by equating the fugacity of water (labeled component 2; helium is component 1) in the equilibrium solid and vapor phases. Neglecting the tiny solubility of helium in ice and the compressibility of ice, we have

$$p_2^{\text{sat}} \phi_2^{\text{sat}} \exp\left[\frac{v_{\text{ice}}(p - p_2^{\text{sat}})}{RT}\right] = y_2 \phi_2 p. \quad (13)$$

The left side of Eq. (13) gives the fugacity of pure ice at the experimental temperature  $T$  and pressure  $p$ . The vapor pressure of ice at  $T$  is  $p_2^{\text{sat}}$ , which we take from Wagner *et al.*<sup>32</sup> The fugacity coefficient of water vapor in equilibrium with ice at saturation is  $\phi_2^{\text{sat}}$ , which we take from the NIST database for water properties.<sup>33</sup> The exponential term is the Poynting correction for the effect of pressure on the solid fugacity; the molar volume of ice  $v_{\text{ice}}$  is from Wexler<sup>34</sup> and  $R$  is the molar gas constant. The measured mole fraction of water in the vapor is  $y_2$ . The only unknown in Eq. (13) is  $\phi_2$ , the fugacity coefficient of water in the gas mixture. If we use the virial expansion in its pressure form and truncate after the second virial coefficient (which is generally superior to similarly truncating the volume form),<sup>35</sup>  $\phi_2$  is given by

$$\ln \phi_2 = (2y_1 B_{12} + 2y_2 B_{22} - B_{\text{mix}}) \frac{p}{RT}, \quad (14)$$

where  $B_{\text{mix}} = y_1^2 B_{11} + 2y_1 y_2 B_{12} + y_2^2 B_{22}$  is the second virial coefficient of the mixture. The second virial coefficients of pure helium and water,  $B_{11}$  and  $B_{22}$ , are taken from Hurly and Moldover<sup>36</sup> and Hill and MacMillan,<sup>37</sup> respectively. Equations (13) and (14) can be solved for  $B_{12}$  from a measurement of  $y_2$  at any temperature and pressure.

Iomtev *et al.*<sup>31</sup> reported measured values of  $y_2$  and associated uncertainties  $\sigma_2$  at several pressures along isotherms. We did not consider points at pressures below 1 MPa, because their uncertainty in  $y_2$  produced enormous uncertainty in  $B_{12}$ . Similarly, the highest pressure considered was 5.07 MPa on the grounds that neglected higher-order terms in the virial expansion would be too large at higher pressures. A few points in another table (from a different experimental setup) with much larger uncertainties were also omitted. This left between one and seven data points at each of seven different temperatures. Values of  $B_{12}$  were fitted at each temperature, minimizing the sum of squares of the deviation in  $y_2/\sigma_2$ . The results are listed in Table V.

Uncertainties in  $B_{12}$  (as standard uncertainties with coverage factor 2) were estimated by a parametric bootstrap method.<sup>38</sup> Simulated data were generated based on the uncertainties  $\sigma_2$ , which we assumed signified one standard deviation. The uncertainties in  $B_{12}$ , shown in Table V, are probably an underestimate in that they account only for uncertainty in the measurement of  $y_2$ . Probably the most im-

TABLE V. Experimental second virial coefficients derived from data of Iomtev *et al.*<sup>a</sup> Uncertainty,  $\Delta B$  (standard uncertainty with a coverage factor of 2), computed as described in the text. Temperatures are given in K,  $B_{12}(T)$  and  $\Delta B$  in  $\text{cm}^3 \text{mol}^{-1}$ .

$T$	$B_{12}$	$\Delta B$
208.16	-5.2	56.1
223.16	7.1	15.9
233.16	12.9	8.5
243.16	14.4	5.4
253.15	15.6	7.6
263.15	15.7	7.6
271.15	16.7	5.0

<sup>a</sup>Reference 31.

portant additional uncertainties arise from the neglect of higher-order virial terms and, at lower temperatures, uncertainty in  $p_2^{\text{sat}}$ .

### B. Calculated second virial coefficients

The second virial coefficient has been calculated using the methods outlined in Sec. II E. The H<sub>2</sub>O orientation is sampled using a two-dimensional Sobol sequence of 16 384 ( $2^{14}$ ) points and the virial coefficient components [see Eqs. (10)–(12)] are calculated using radial quadrature of orientationally averaged results out to 45  $a_0$  in steps of 0.01  $a_0$ . The uncertainties resulting from this quadrature scheme are estimated to vary between about 0.6% at 100 K and about 0.01% at 2000 K, very much smaller than those associated with uncertainties in the potential (see below).

The experimental results and those using Surface III are given in Tables V and VI. Experimental and calculated results are also shown in Fig. 6. The theoretical uncertainties are estimated by using Surface I as an upper bound and a

TABLE VI. Calculated second virial coefficients for Surface III. Temperatures are given in K; all  $B_{12}(T)$  components and the uncertainty in the total second virial coefficient,  $\Delta B$ , are given in  $\text{cm}^3 \text{mol}^{-1}$ . The method used to estimate  $\Delta B$  is described in the text.

$T$	$B_{\text{class}}$	$B_{\text{quant}}^{\text{rot}}$	$B_{\text{quant}}^{\text{trans}}$	$B_{\text{tot}}$	$\Delta B$
100	3.259	0.222	1.385	4.865	3.5
125	7.955	0.141	0.971	9.066	2.9
150	10.83	0.099	0.734	11.67	2.5
175	12.73	0.075	0.584	13.39	2.2
200	14.05	0.060	0.481	14.59	2.0
225	14.99	0.049	0.406	15.45	1.8
250	15.69	0.041	0.350	16.08	1.7
275	16.21	0.036	0.306	16.55	1.6
300	16.60	0.031	0.272	16.90	1.5
400	17.43	0.020	0.183	17.63	1.3
500	17.68	0.015	0.136	17.83	1.1
600	17.68	0.012	0.107	17.80	1.0
700	17.57	0.009	0.087	17.67	0.9
800	17.40	0.008	0.073	17.48	0.8
900	17.21	0.007	0.063	17.28	0.8
1000	17.01	0.006	0.055	17.07	0.7
1200	16.59	0.005	0.043	16.64	0.7
1400	16.19	0.004	0.035	16.23	0.6
1600	15.82	0.003	0.030	15.85	0.6
1800	15.46	0.003	0.025	15.49	0.5
2000	15.14	0.002	0.022	15.16	0.5

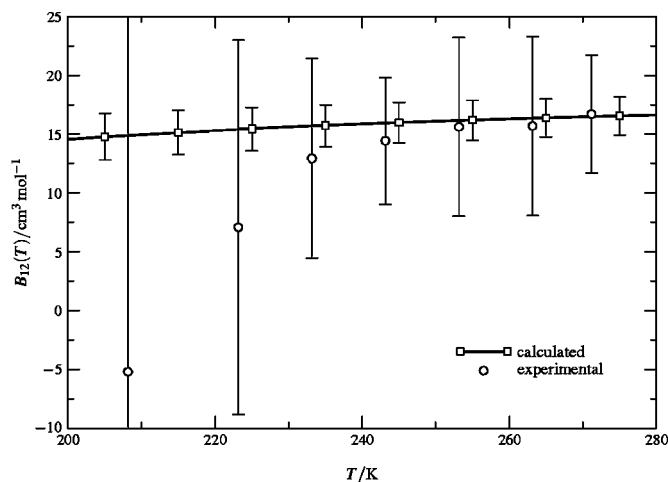


FIG. 6. Comparison of experimental and calculated  $B_{12}(T)$  data. The estimation of the calculated error bars is described in the text. The experimental error bar at 208.16 K is  $\pm 56.1 \text{ cm}^3 \text{ mol}^{-1}$ .

fourth fitted surface (Surface IV, with  $k=1.125$ ) as a lower bound. (The minimum energy of Surface IV is about  $-185 \mu E_h$ , i.e., about  $25 \mu E_h$  lower in energy than our best estimate using Surface III.) The large differences between these three surfaces lead to uncertainties that are probably overestimates; we note that the error in the global minimum energy for Surface III is likely to be much smaller than the differences between Surfaces III and I, and Surfaces III and IV. The use of the Surface I results is, however, conceptually appealing because this surface is not calibrated using any supermolecule results. The  $\pm$  uncertainties are reasonably symmetric, so only their mean is given in Table VI.

The calculated data are plotted alongside the experimental data, which are only available over a small temperature range, in Fig. 6. It is apparent that the magnitudes of the experimental uncertainties are such that the experimental data are incapable of providing a quantitative account of the behavior of  $B_{12}$  over this temperature range. In particular, the calculated values show that  $B_{12}$  varies much less over this

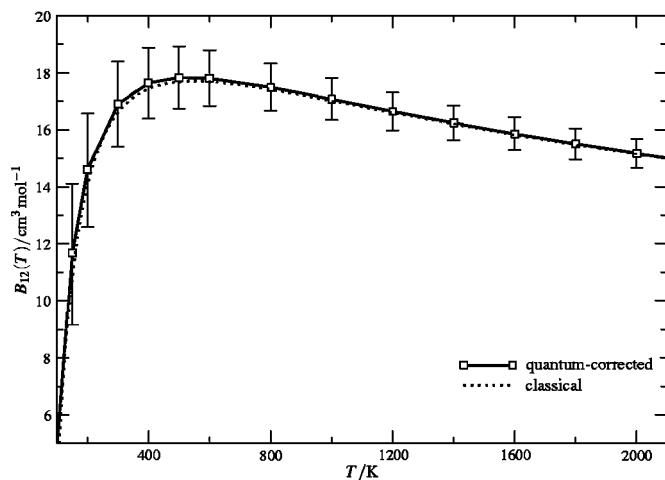


FIG. 7. Calculated classical and quantum-corrected second virial coefficients,  $B_{12}(T)$ . The estimation of the calculated error bars is described in the text.

TABLE VII. Parameters for an analytic approximation of  $B_{12}(T)$ . The  $a_i$  are given in  $\text{cm}^3 \text{ mol}^{-1}$  and the  $b_i$  are dimensionless; the functional form is given in Eq. (15).

$i$	$a_i$	$b_i$
1	55.57	-0.347
2	-59.25	-0.85
3	13.32	-1.45
4	-4.767	-2.1

temperature range than otherwise might have been inferred from the experimental data, even though the calculated values lie within the experimental error bars. The calculated uncertainties (which are probably too large) are significantly smaller than the experimental ones, especially for the lower temperature points, and this demonstrates the value of calculating  $B_{12}$  when its experimental determination is difficult.

The temperature range that we consider (100–2000 K) is determined by the applications mentioned in the Introduction and is much larger than that accessible experimentally. Additional calculated values of  $B_{12}$  are shown in Fig. 7 and the components are given in Table VI. It is apparent that the first-order quantum effects play only a minor role even at the lowest temperature reported—at 100 K, the rotational and translational components contribute about 0.22 and 1.4  $\text{cm}^3 \text{ mol}^{-1}$  to the quantum-corrected value of  $B_{12}$ ; by 150 K, these contributions have been approximately halved and represent 0.85% and 6.3% of the total value, respectively. We attribute the dominance of the translational quantum correction to the weak angular anisotropy of the potential-energy surface, and the main contribution to this component arises through the radial forces. While the quantum contributions are not insignificant, they represent contributions that are smaller than the error estimates in the  $B_{12}$  results due to the uncertainties in the potential-energy surface; higher-order corrections can be expected to be considerably smaller, and it does not seem worthwhile determining them at present.

### C. Analytic representation of the second virial coefficient

For practical use, it is desirable to be able to calculate  $B_{12}$  without having to perform the numerical evaluations of Eqs. (10)–(12). We therefore fit a function to the results of our calculations:

$$B_{12}(T) \approx \sum_{i=1}^4 a_i (T^*)^{b_i}, \quad (15)$$

where  $T^* = T/100 \text{ K}$  and the coefficients  $a_i$  and  $b_i$  are given in Table VII. Equation (15) fits the results from 100 K to 2000 K to within  $0.01 \text{ cm}^3 \text{ mol}^{-1}$ , which is comparable with the uncertainty of the numerical integrations at high  $T$ . It also extrapolates in a physically reasonable manner at higher and lower temperatures, although we recommend its use only for the stated range.

## V. CONCLUSIONS

We develop a new potential-energy surface for the weakly bound water-helium complex using perturbation theory methods, and calibrate the interaction energy at the global minimum to reproduce an estimate of the complete basis set limit at the CCSD(T) level of theory. The global minimum has the helium atom in the plane of the water molecule with the O→He vector nearly perpendicular to the molecular symmetry axis, and this is attributed to competing effects of maximizing the dispersion interaction and minimizing the repulsion with the lone pairs.

An analytic fit of the potential-energy surface is used to calculate the cross second virial coefficient,  $B_{12}(T)$ , and experimental values are extracted from limited data for the solubility of ice in helium. The theoretical calculations can be considered superior to the experimental data as the estimated uncertainties in  $B_{12}(T)$  are found to be much smaller than those derived from the experimental data. In addition, the experimental data are only available over a narrow range of temperatures (208.16–271.15 K), whereas the theoretical calculations can be performed at any temperature. We emphasize that the calculation of  $B_{12}(T)$  is the primary consideration here, in contrast to the common practice of using experimental second virial coefficient data to validate a potential-energy surface. Additional applications of the potential to spectroscopic or scattering calculations could be used to further test its accuracy.

The quantum corrections to  $B_{12}(T)$  have been evaluated using a semi-classical expansion to first order in  $\hbar^2$  and are found to contribute about 7% at 150 K. The translational component is about an order of magnitude larger than the rotational component at all temperatures, and this is attributed to weak angular anisotropy in the potential-energy surface. However, for all temperatures, the magnitude of the quantum correction is significantly smaller than the uncertainty due to the potential-energy surface.

## ACKNOWLEDGMENTS

The authors thank E. W. Lemmon for assistance in fitting Eq. (15), and K. J. Coakley for advice on statistical evaluation of the uncertainties associated with the data given in Table V. The GAUSSIAN 94 calculations were performed on Columbus, part of the U.K. Computational Chemistry Facility. The author M.P.H. thanks the Leverhulme Trust for financial support.

<sup>1</sup>M. P. Hodges and R. J. Wheatley, *J. Chem. Phys.* **114**, 8836 (2001).

<sup>2</sup>F.-M. Tao, Z. Li, and Y.-K. Pan, *Chem. Phys. Lett.* **255**, 179 (1996).

<sup>3</sup>S. Green, D. J. DeFrees, and A. D. McLean, *J. Chem. Phys.* **94**, 1346 (1991).

<sup>4</sup>S. Maluendes, A. D. McLean, and S. Green, *J. Chem. Phys.* **96**, 8150 (1992).

<sup>5</sup>J. Brudermann, P. Lohbrandt, U. Buck, and V. Buch, *J. Chem. Phys.* **112**, 11038 (2000).

<sup>6</sup>R. W. Hyland and A. Wexler, *ASHRAE Trans.* **89**, 520 (1983).

<sup>7</sup>S. Hasegawa and J. W. Little, *J. Res. Natl. Bur. Stand., Sect. A* **81**, 81 (1977).

<sup>8</sup>R. S. Davis, *Metrologia* **29**, 67 (1992).

<sup>9</sup>K. P. Birch and M. J. Downs, *Metrologia* **30**, 155 (1993).

<sup>10</sup>M. R. Patel, J. C. Holste, K. R. Hall, and P. T. Eubank, *Fluid Phase Equilib.* **36**, 279 (1987).

<sup>11</sup>A. H. Harvey, in "Steam, Water and Hydrothermal Systems: Physics and Chemistry Meeting the Needs of Industry," edited by P. R. Tremaine, P. G. Hill, D. E. Irish, and P. V. Balakrishnan, *Proceedings of the 13th International Conference on the Properties of Water and Steam* (NRC Research, Ottawa, 2000), p. 571.

<sup>12</sup>E. M. Mas and K. Szalewicz, *J. Chem. Phys.* **104**, 7606 (1996).

<sup>13</sup>*The GNU Scientific Library*, <http://sources.redhat.com/gsl/>, 0.9 edn. (2001).

<sup>14</sup>R. A. Kendall, T. H. Dunning, and R. J. Harrison, *J. Chem. Phys.* **96**, 6796 (1992).

<sup>15</sup>D. E. Woon and T. H. Dunning, *J. Chem. Phys.* **100**, 2975 (1994).

<sup>16</sup>A. J. Thakkar, *J. Chem. Phys.* **75**, 4496 (1981).

<sup>17</sup>K. T. Tang and J. P. Toennies, *J. Chem. Phys.* **80**, 3726 (1984).

<sup>18</sup>D. J. Margolias and W. J. Meath, *J. Chem. Phys.* **68**, 1426 (1978).

<sup>19</sup>M. J. Frisch, G. W. Trucks, H. B. Schlegel *et al.*, GAUSSIAN 94, Revision E.3, Pittsburgh, PA, 1995.

<sup>20</sup>Certain commercial products are identified in this paper, but only in order to adequately specify the procedure. Such identification neither constitutes nor implies recommendation or endorsement by either the U.S. government or the National Institute of Standards and Technology.

<sup>21</sup>R. J. Wheatley and J. B. O. Mitchell, *J. Comput. Chem.* **15**, 1187 (1994).

<sup>22</sup>M. P. Hodges and R. J. Wheatley, *Chem. Phys. Lett.* **326**, 263 (2000).

<sup>23</sup>H.-J. Werner, P. J. Knowles, R. D. Amos *et al.*, MOLPRO, a package of ab initio programs, University of Birmingham, U.K., 1997.

<sup>24</sup>S. F. Boys and F. Bernardi, *Mol. Phys.* **19**, 553 (1970).

<sup>25</sup>C. G. Gray and K. E. Gubbins, *Theory of Molecular Fluids*, Fundamentals Vol. 1 (Clarendon, Oxford, 1984).

<sup>26</sup>See EPAPS Document No. E-JCPSA6-115-005148 for FORTRAN source code and documentation for the intermolecular potential described in this paper. This document may be retrieved via the EPAPS homepage (<http://www.aip.org/pubservs/epaps.html>) or from <ftp.aip.org> in the directory /epaps/. See the EPAPS homepage for more information.

<sup>27</sup>R. Moszynski, P. E. S. Wormer, B. Jeziorski, and A. van der Avoird, *J. Chem. Phys.* **101**, 2811 (1994).

<sup>28</sup>A. Bagno, *J. Chem. Soc., Faraday Trans.* **94**, 2501 (1998).

<sup>29</sup>R. C. Cohen and R. J. Saykally, *J. Chem. Phys.* **98**, 6007 (1993).

<sup>30</sup>M. P. Hodges, R. J. Wheatley, and A. H. Harvey (unpublished).

<sup>31</sup>M. B. Iomtev, V. G. Piskunov, and V. L. Kadzhayev, *Tables of the National Standard Reference Data Service of the USSR*, Tech. Rep. R243-86 (All-Union Research Center of Standard and Reference Data, Moscow, 1987), cited in V. A. Rabinovich and V. G. Beketov, *Moist Gases. Thermodynamic Properties* (Begell House, New York, 1995).

<sup>32</sup>W. Wagner, A. Saul, and A. Pruss, *J. Phys. Chem. Ref. Data* **23**, 515 (1994).

<sup>33</sup>A. H. Harvey, A. P. Peskin, and S. A. Klein, *NIST/ASME Steam Properties, NIST Standard Reference Database 10, Version 2.2* (National Institute of Standards and Technology, Gaithersburg, MD, 2000).

<sup>34</sup>A. Wexler, *J. Res. Natl. Bur. Stand., Sect. A* **81**, 5 (1977).

<sup>35</sup>J. M. Prausnitz, R. N. Lichtenthaler, and E. Gomes de Azevedo, *Molecular Thermodynamics of Fluid-Phase Equilibria*, 3rd ed. (Prentice Hall, Upper Saddle River, NJ, 1999).

<sup>36</sup>J. J. Hurly and M. R. Moldover, *J. Res. Natl. Inst. Stand. Technol.* **105**, 667 (2000).

<sup>37</sup>P. G. Hill and R. D. C. MacMillan, *Ind. Eng. Chem. Res.* **27**, 874 (1988).

<sup>38</sup>B. Efron and R. J. Tibshirani, *An Introduction to the Bootstrap*, No. 57 in Monographs on Statistics and Applied Probability (CRC, Boca Raton, 1994).